REPORT DOCUMENTATION PAGE	Form Approved OMB No. 0704-0188

PLEASE DO NOT RETURN YOUR FORM TO THE ABOVE ADDRESS.

1. REPORT DATE *(DD-MM-YYYY)*	2. REPORT TYPE	3. DATES COVERED *(From - To)*
07-14-03	Final Technical Report	Jan. 1, 2000 - June 30, 2003

4. TITLE AND SUBTITLE
Creep Behavior of Polymer Precursor Derived Si3N4/SiC Nanocomposites
Final Technical Report

5a. CONTRACT NUMBER

5b. GRANT NUMBER
N00014-00-1-0186

5c. PROGRAM ELEMENT NUMBER

6. AUTHOR(S)
Mukherjee, Amiya K.

5d. PROJECT NUMBER

5e. TASK NUMBER

5f. WORK UNIT NUMBER

7. PERFORMING ORGANIZATION NAME(S) AND ADDRESS(ES)
Department of Chemical Engineering and Materials Science
University of California
One Shields Avenue
Davis, CA 95616

8. PERFORMING ORGANIZATION REPORT NUMBER

9. SPONSORING/MONITORING AGENCY NAME(S) AND ADDRESS(ES)
Asuri K. Vasudevan
Office of Naval Research
Ballston Centre Tower One
800 North Quincy Street
Arlington, VA 22217-5660

10. SPONSOR/MONITOR'S ACRONYM(S)
ONR

11. SPONSOR/MONITOR'S REPORT NUMBER(S)

12. DISTRIBUTION/AVAILABILITY STATEMENT
Approved for Public Release; distribution unlimited

13. SUPPLEMENTARY NOTES

14. ABSTRACT
The creep properties of silicon nitride/silicon carbide nanocomposites were studied in compression. The material was processed using the route of pyrolysis of a polymer precursor. The extraordinary low creep rate that was experimentally measured in this project was obtained by primarily minimizing the presence of intergranular glassy phase.

15. SUBJECT TERMS
silicon nitride/silicon carbide, nanocomposite, polymer precursor, creep, microstructure

16. SECURITY CLASSIFICATION OF:			17. LIMITATION OF ABSTRACT	18. NUMBER OF PAGES	19a. NAME OF RESPONSIBLE PERSON
a. REPORT	b. ABSTRACT	c. THIS PAGE		20	Amiya K. Mukherjee
					19b. TELEPHONE NUMBER *(Include area code)* 530-752-1776

OFFICE OF NAVAL RESEARCH

FINAL TECHNICAL REPORT

Contract Information

Contract Number	N00014-00-1-0186
Title of Research	Creep Behavior of Polymer Precursor Derived Si_3N_4 /SiC Nanocomposites
Principal Investigator	Amiya K. Mukherjee
Organization	Department of Chemical Engineering and Materials Science, University of California, Davis

Technical Objectives

In the first half of this three-year project, we have succeeded in processing silicon nitride/silicon carbide nanocomposites with a wide variety of microstructures. In-situ pyrolysis/consolidation follows by crystallization was the focus of FY 2001. With this approach, high-density bulk amorphous Si-C-N materials have been produced; silicon nitride/silicon carbide nano-nanocomposites were derived by crystallization of the amorphous ceramics. Spark plasma sintering as a complimentary processing route, silicon nitride and silicon carbide micro-nanocomposites were produced with short sintering time and low temperature. The focus of FY2002 was batch production of testing materials and property evaluation of these materials.

Entering the third fiscal year, the major objective was shifted to optimizing the processing technology, based on the work completed in the previous two years. The specific technical objective in this year include:

- Optimization of the processing technique of Spark Plasma Sintering. The target is to decrease the amount of sintering additive, by which the creep resistance of the materials is expected to improve.
- High pressure sintering is also attempted, in an effort to produce nano-nano composites that has the potential for enhanced superplasticity.
- Preliminary creep tests to establish the guideline for the next phase of the project. We have established the stress-dependence of the creep rate, the activation energy of the rate controlling process, and analyzed the microstructure both before and after deformation.

Technical Approach

SPS of Si-C-N

In the earlier reports to ONR for of FY 2000 and 2001, it was demonstrated that spark plasma sintering (SPS) process, in which the powder particle surfaces are easily cleaned and activated, material transfer at both the micro and macro levels are promoted, so a high quality sintered compact is obtained at a lower temperature and in a shorter time than with conventional processes. SPS of the amorphous Si-C-N powder derived from pyrolysis of polymer precursor, along with similar level of oxide sintering aid (e.g., 8wt% Y_2O_3 or 5 wt% $MgAl_2O4$), can produce dense sintered micro-nano type composites at 1600°C within 10 minutes. The creep testing of the micro-nano composites show that in spite of the higher creep resistance observed in these materials, the creep mechanism is likely to be similar as in conventional silicon nitride monoliths, which is solution precipitation of the crystalline phases through the glassy grain boundary phase. Therefore, the prospect of further improving the creep property lies in the decrease of the amount of sintering additive.

In order to examine the effect of additive amount on the sintering behavior, microstructure as well as property of the materials, 1, 3, 5, 8 wt% Y_2O_3 was added to amorphous Si-C-N from 1450°C/4hr/1 atm. N_2 pyrolysis of Ceraset SN polymer precursor. Powder mixtures were high energy ball-milled under nitrogen protection for 24 hours, with silicon nitride milling media. The powders were installed into a graphite die/punch assembly with an inner diameter of 19mm. SPS was conducted in vacuum. After a pressure of 63 MPa was applied, a pulsing electric current passing through the die/punch assembly heats the sample up to 600°C in 2 minutes. The heating rate was controlled at 100°C/minute at higher temperatures up to the final sintering temperature. The temperature was held at the sintering point for 10 minutes before the pulsing current was turned off, and the assembly was allowed to cool down along with the release of sintering pressure.

Attempts were also made to sinter the material without using any additive. If the sintering is successful, it is expected that the technique would provide material with the best creep resistance, owing to the lack of an effective glassy grain boundary phase. The powder manipulation and sintering follows the same procedure as what was introduced above, only that the sintering time is extended to 30 minutes.

Synthesis of Si-B-C-N composites

The process of making the Si_3N_4/SiC/BN triphasic nanocomposite is schematically shown as the flow chart in Fig. 1.

Instead of developing special polyborocarbosilazane polymer precursor that can be pyrolyzed into Si-B-C-N ceramics, we have taken another approach: using a well-documented commercial precursor for Si-C-N ceramics, Ceraset SN polyureasilazane, react it with decaborane to form precursors and can be pyrolyzed into Si-B-C-N amorphous ceramics. As compared with the other routes that develop special boron-containing precursors, the present approach is much less requiring for instrumentation and also for processing control. Furthermore, the ceramics from Ceraset SN is also noted for the excess carbon (hence insufficient silicon) after crystallization,

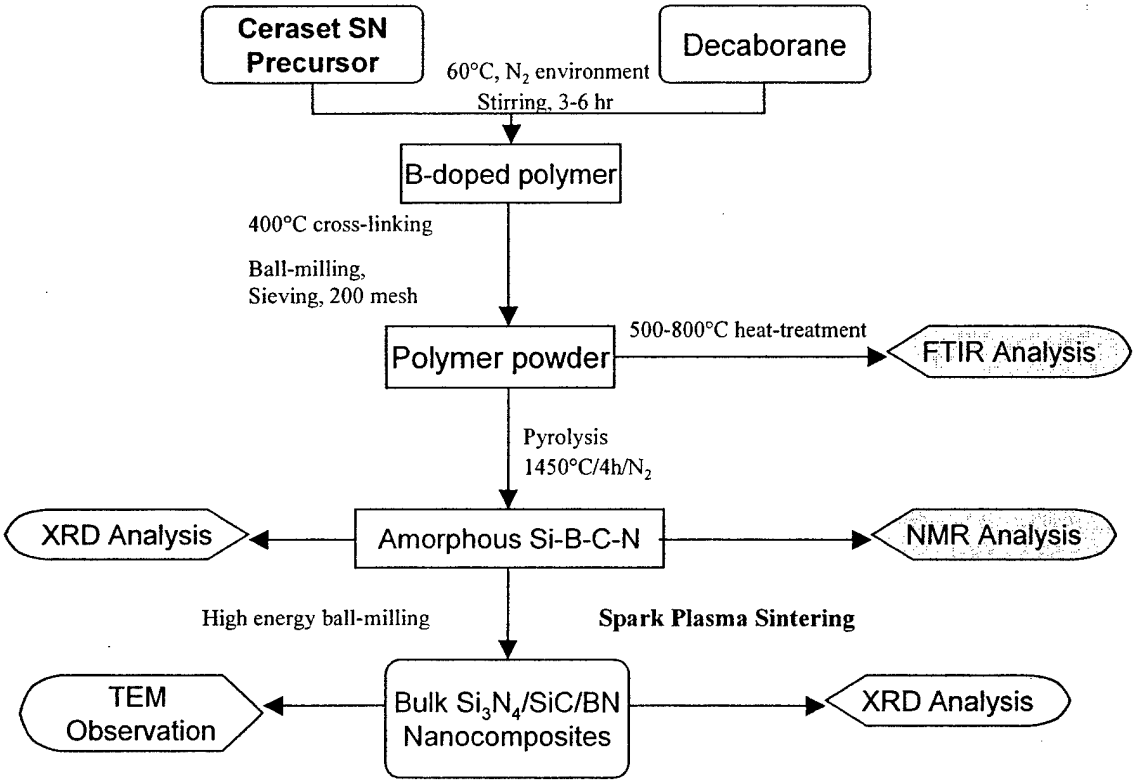

Fig. 1 Flow chart for producing Si-B-C-N system nanocomposites

which is detrimental for the thermal stability of the material. Decaborane contains only boron and hydrogen as component elements, incorporation of boron might be able to compensate for the excess carbon and thus bring the material close to chemical stoichiometry and therefore enhance the thermal stability of the crystallized material.

The liquid Ceraset polymer was mixed with different amounts of decaborane (Alfa Aesar Inc., Ward Hill, Maine) to obtain batches of precursors with varied boron content. The mixtures are further added with 0.5wt% dicumyl peroxide (98%, Aldrich Chemical Company, Inc., Milwaukee, WI) as cross-linking catalyst, and stirred in nitrogen atmosphere for 4-6 hours, the temperature of the mixture was maintained at 60-80°C. Cross-linking was conducted by bringing the temperature to 400°C and holding the temperature for one hour. The infusible solids that resulted from cross-linking were then ball-milled to 200 mesh powders. Pyrolysis was conducted at 1400°C for 4 hours in a furnace with flowing nitrogen gas.

Altogether four batches of powders were made; they were doped with 2wt%, 5wt%, 10wt% and 20wt% of decaborane. The batches will be designated as 2B, 5B, 10B, and 20B hereafter in this paper. The pyrolysis process of all the batches of powders were examined by transmission mode FTIR spectroscopy of the powders of the as cross-linked state and that heat-treated to 500, 600, 700 and 800°C for one hour. For crystallization studies, the 1450°C pyrolyzed powders were heated to 1550, 1650, 1750, 1800 and 1850°C and maintained at temperature for 2 hours. All the heat-treatments were done under flowing nitrogen atmosphere. To serve as a reference, the polymer without boron doping was also treated under the same circumstances. X-ray diffraction was conducted to all the heat-treated powders. ^{29}Si and ^{11}B solid-state nuclear magnetic resonance (NMR) spectroscopy examinations were conducted on all the 1450°C-treated powders, as well as the batch 10B powders subjected to 1550-1850°C heat-treatment, applying the magic angle spinning technique (MAS) with spinning rate of 16kHz. ^{29}Si spectra were also recorded for the undoped ceramic heat-treated at 1550 and 1650°C.

Manipulation and sintering of the boron-containing amorphous powders follow the same procedure as the Si-C-N materials. No sintering additive was applied.

HPS of Si-C-N with high level of additive

This approach was taken as a complimentary technique to produce nano-nano silicon nitride/ silicon carbide composite at high additive levels.

The cross-linked infusible polymer was ball-milled into a 200-mesh powder, and then pyrolyzed at 1450°C for 4 hours in nitrogen. The resultant amorphous Si-N-C powder was mixed with 8wt% Y_2O_3 by high-energy ball milling.

Compaction was carried out in a Boyd-England apparatus. A schematic diagram of the set-up of the furnace assembly is shown in Fig.2. A green compact was first prepared by uniaxial compression of amorphous powder at ~15MPa. This pellet was then placed at the midpoint of the furnace assembly.

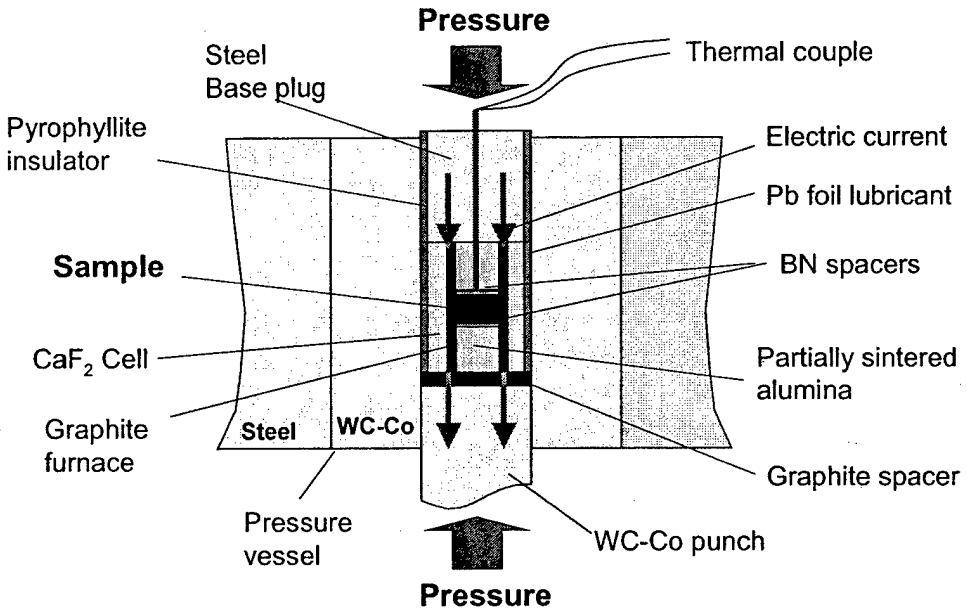

Fig. 2 - Schematic illustration of the assembly used for high-pressure sintering

The furnace assembly is comprised of a 32mm long and 6.4mm inner diameter graphite furnace, surrounded by a sheath of CaF_2 and Pb foil. The CaF_2 layer crumbles under pressure and acts as a pressure-transmitting medium. Once crushed it transforms uniaxial pressure into quasi-hydrostatic pressure. The Pb foil acts as a lubricant for the furnace assembly during the push-out after the test. The remaining volume of the furnace is filled by semi-sintered Al_2O_3 filler rod. A D type thermocouple (W/Re) was placed at the top of the sample and temperature was regulated using a Eurotherm controller. Sintering was performed by applying a pressure of 2GPa on the sample then heating at a rate of 150°C/min to 1400-1600°C. Once at temperature, samples were held for 10 minutes before the pressure was reduced to ~0.5GPa. The temperature and remaining pressure were then allowed to ramp down simultaneously.

Results

SPS kinetics-effect of additive level

Sintering kinetics offer an approach to understand the sintering mechanism from the consolidation behavior. Examples of sintering curves are shown in Fig. 3. SPS kinetics appear to follow the classic description of the mechanism of liquid phase sintering, which is composed of three stages: particle rearrangement, solution-precipitation, followed by solid-state sintering. Sintering at high liquid level (high additive content) brings about fast sintering through particle

rearrangement and solution-precipitation, which is sufficient to consolidate the material. This is manifested by the abrupt decrease of displacement rate following the summit of the peak. While at low liquid levels a final stage of solid state sintering is indispensable to densify the solid skeleton. Densification based on solid-state diffusion, as compared with liquid phase sintering, is much slower in kinetics; the extended shoulder after the sintering peak is a result of the participation of this mechanism.

Decreasing or elimination of oxide sintering aids decreases the significance of liquid phase sintering. But with the participation of solid-state sintering, possibly accelerated by the pulsing electric field, the amorphous powders can be sintered by SPS at low temperature to near full density.

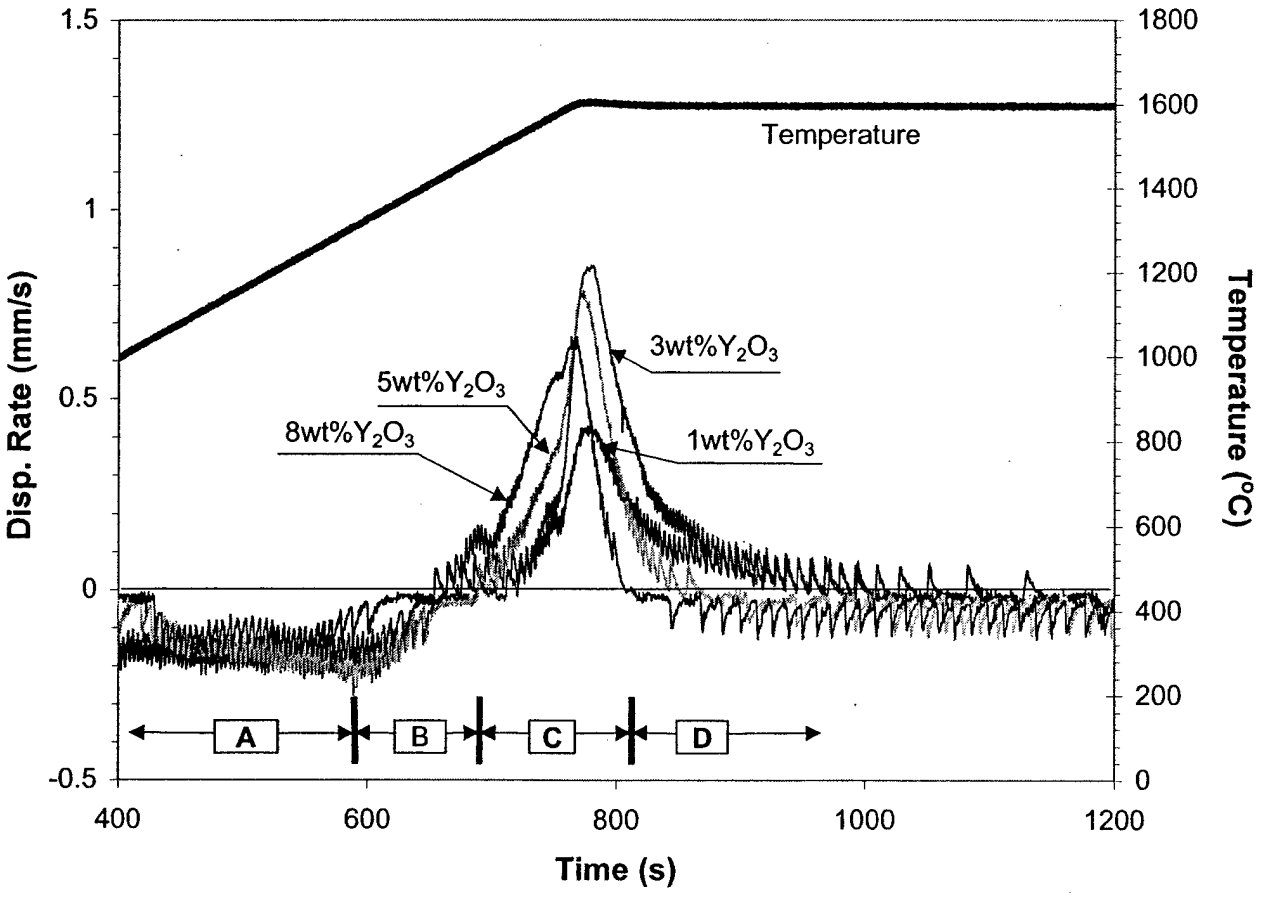

Fig. 3 Measured SPS sintering curves showing effect of additive level

SPS produced Si_3N_4/SiC nanocomposites –Micro-nano to nano-nano

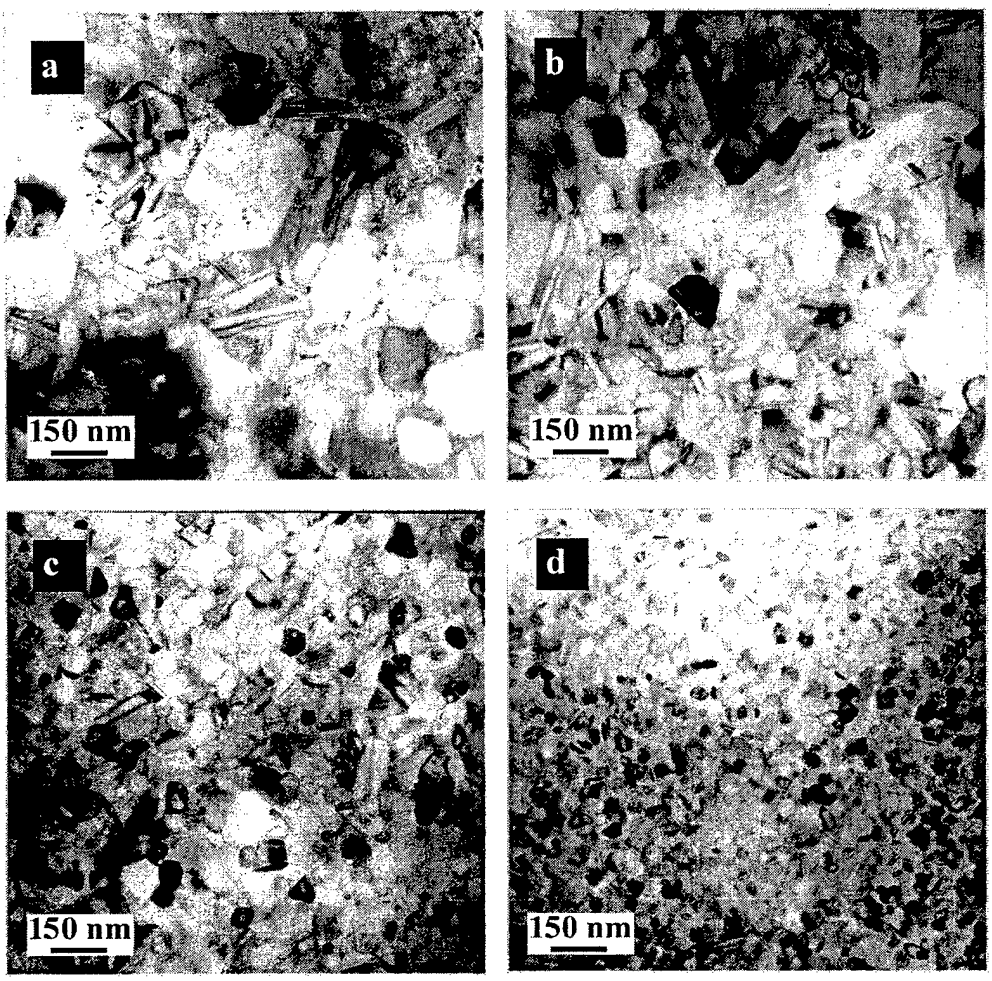

Fig. 4 Microstructure of nanocomposites sintered by SPS at 1600°C/10min with (a) 8wt% Y_2O_3 (b) 5wt% Y_2O_3 (c) 3wt% Y_2O_3 (d) 1wt% Y_2O_3

SPS of the pyrolysis-derived Si-C-N can consolidate Si_3N_4/SiC to high density at virtually any additive level. It was found that the level of additive has a profound effect on microstructure. The microstructures of the materials sintered with 1-8wt% at 1600°C/10min as observed by TEM are shown in Fig. 4. With 8wt%Y_2O_3, the microstructure is a typical micro-nano type as also achieved by conventional hot-pressing. The mean grain size of the matrix (composed of silicon nitride and intergranular SiC, intragranular SiC was not included in the calculation) is about 146nm for this material (Fig. 4(a)). Lowering the yttria amount to 5wt% leads to microstructure that essentially also fits the above description of micro-nano composites. Although the mean-grain-size is already within the 100nm limit (~86nm), there is a significant part of the grains that

are about 200nm (Fig. 4(b)). Decreasing of yttria amount to 3wt% fundamentally changed the appearance of the microstructure. There are no more large silicon nitride grains that enclose SiC particles, the microstructure is a homogenous dual-phase mixture of silicon nitride and silicon carbide equiaxial grains, and the mean grain-size is about 56nm (Fig. 4(c)). Further decrease of yttria amount to 1wt% results in nano-nano microstructure of silicon nitride and silicon carbide with a grain size of about 38nm (Fig. 4(d)).

Si_3N_4/SiC nanocomposites without additive

The most remarkable achievement by SPS approach is the successful synthesis of Si_3N_4/SiC nano-nano type composites without sintering additive. Notice that conventional silicon nitride cannot be sintered without additive. Complete elimination of oxide additive from the material has been the target for research in silicon nitride for a long time. This achievement is expected to bring major improvement to high temperature properties such as creep resistance, and as we will show later this is, indeed, the case.

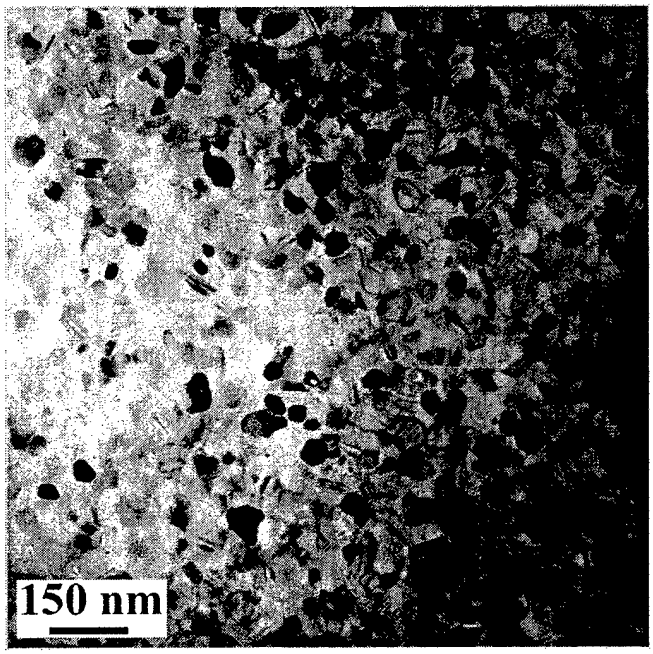

Fig. 5 Nano-nano composite of Si_3N_4/SiC sintered from amorphous Si-C-N without additive by SPS (1600°C/30min)

When the material is sintered without additive, 10 minutes at 1600°C leads to grain size of about 27 nm. With 30 minutes of sintering, the grain size reaches about 40 nm, as shown in Fig. 5.

Electron energy loss spectroscopy (EELS) analysis was conducted to examine the elemental distribution of the nano-nano composites. The EELS mapping of Si, C, N and O is shown in Fig. 7. It is quite clear that the two phases in this material-Si_3N_4 and SiC were randomly mixed with roughly equal grain size. The most important information from these maps is that, oxygen, which

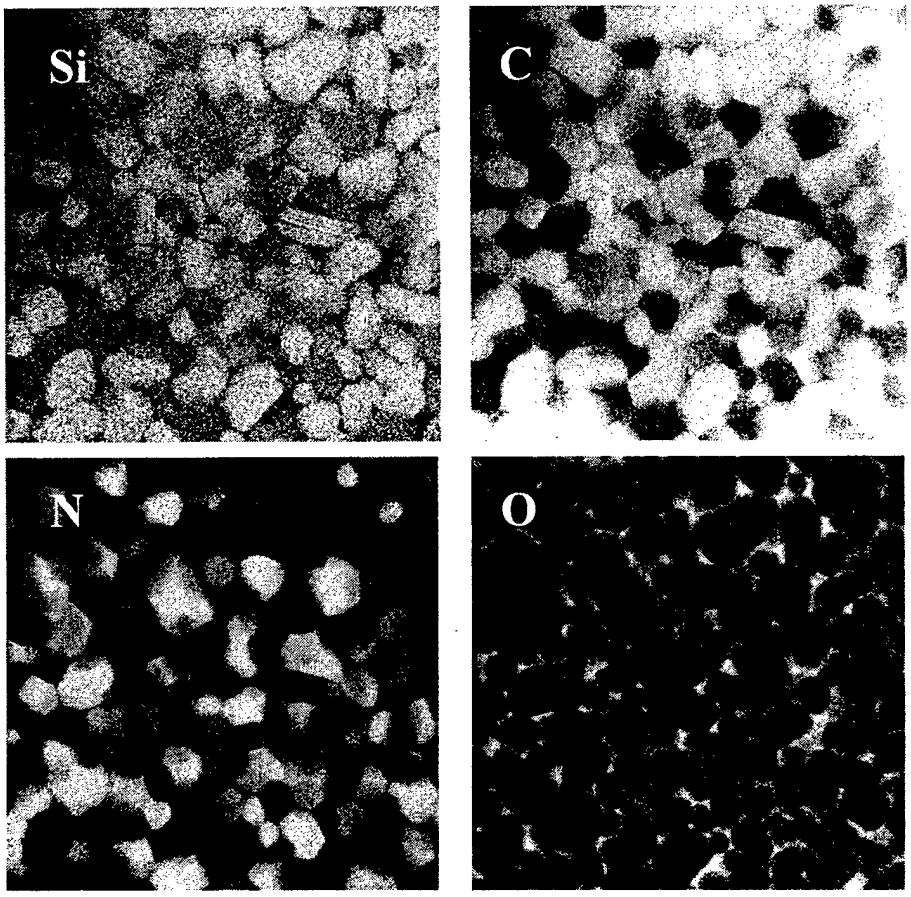

Fig.6 EELS mapping of the nano-nanocomposite SPSed without additive

is the main element responsible for forming glassy grain boundary phases in the absence of metal oxide sintering additives, was found to exist at almost all the intergranular regions, including triple junction pockets and dual-grain boundaries. This is an explicit indication that the oxygen that originally exists mainly at the particle-surface of the starting amorphous powder (in the form of either silica or silicon oxynitride) has diffused into the interior of the particles during sintering, and is sparsely distributed along the grain boundaries.

High-resolution transmission electron microscopy of the grain boundary regions of the similar material as in Fig 5 and Fig. 6, the images are shown in Fig. 7. As in microcrystalline silicon nitride or silicon carbide, most of the glassy grain boundary phase exists at multi-grain junctions, as an example shown in Fig. 7 (c). Some of the dual-grain junctions (grain boundaries) do contain an amorphous layer, as in Fig. 7(b); in this particular example the thickness of amorphous layer is about 1 nm, in accordance with the glassy layer thickness in silicon nitride that contains silica as the only oxide species. The most significant feature in the nano-nano

composites is that they contain a prominent population of grain boundaries that do not have an apparent amorphous layer, as the example in Fig. 7(a) demonstrates.

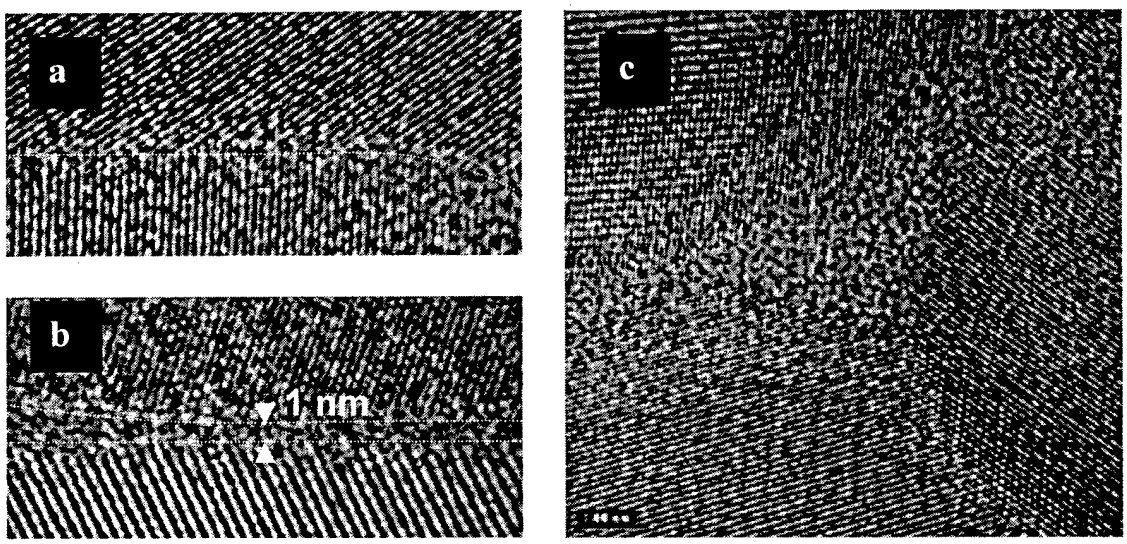

Fig. 7 HRTEM of grain boundary regions of the nanocomposite without additive (a) and (b) grain boundaries (c) triple junction

<u>High pressure sintering (HPS) of Si_3N_4/SiC nano-nano composites</u>

High-applied pressure increases matter-transport (e.g., enhances diffusion) thus enables sintering at low temperatures. A high hydrostatic stress also encourages nucleation for crystallization. These two factors create an ideal condition for sintering nanocrystalline materials from an amorphous powder. In the sections above, we have demonstrated the feasibility of sintering nano-nano composites without additive or with reduced amount of oxide additive. While nano-nano composites with high level of oxides remains evasive, this type of microstructure has a theoretical significance in examining the liquid phase creep mechanism when grain size reaches nano-range. It has its own engineering significance in that it is possible to demonstrate enhanced superplasticity. The current ONR project has succeeded in producing this type of material by HPS.

High pressure sintering of the amorphous Si-C-N doped with 8wt% Y_2O_3 or 5wt%Y_2O_3+5wt%$MgAl_2O_4$ was successfully performed between 1400-1600°C, at a pressure of 1-2 GPa. Within 10 minutes at temperature the materials reach a density level of about 2.9-3.0 g/cm^3. Ceramics sintered at 1400°C are XRD amorphous, but TEM investigation shows small crystals, both of Si_3N_4 and SiC, start to emerge at the boundary regions between the original amorphous Si-C-N particles (Fig. 8(a)). At 1500°C about 70% of the amorphous Si-C-N was

converted into crystalline phases with about 30nm in grain-size, while the internal part of the larger Si-C-N particles remain amorphous (Fig. 8(b)). Sintering at 1600°C/2GPa for ten minutes results in fully crystalline nano-nano composite with a mean grain-size of about 40nm, as shown in Fig. 8(c). HRTEM conducted to the grain boundaries found wide-range distribution of grain boundary thickness, which is assignable to the nonequilibrium condition of the grain boundaries. The yttrium containing oxynitride glassy phase was found to be distributed mainly in grain-boundary triple junction pockets.

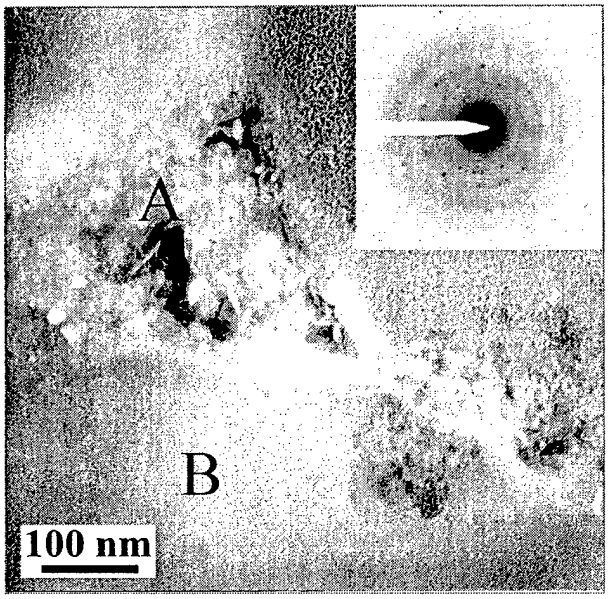

(a)

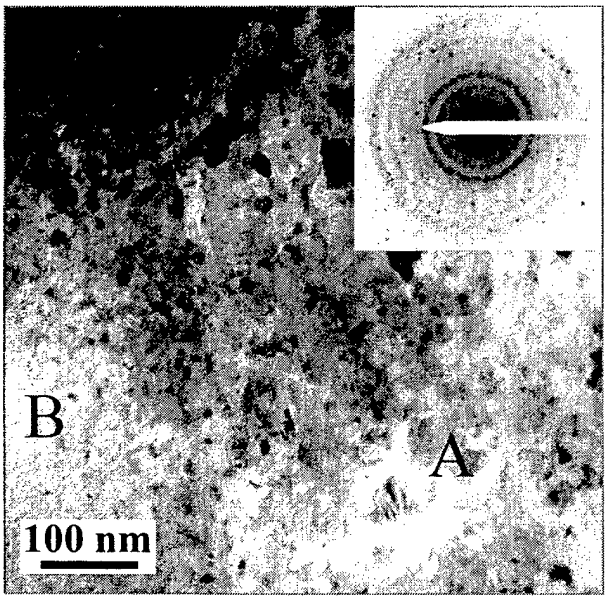

(b)

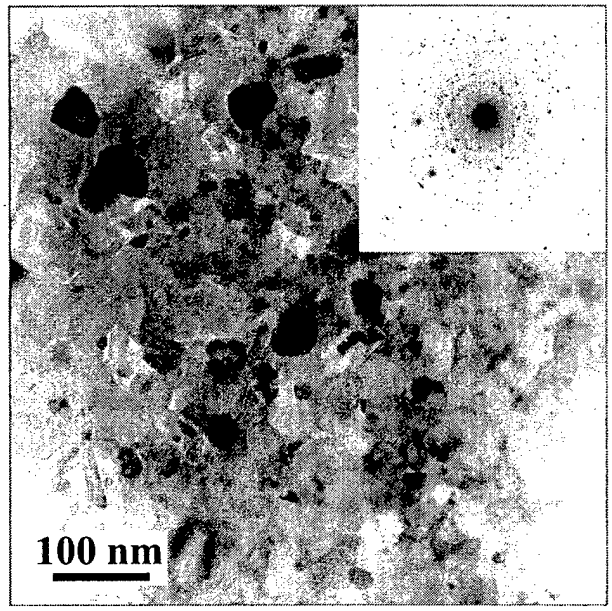

(c)

Fig. 8 Microstructure of composites obtained by high pressure sintering, (a)-(c) represents sintering temperature of 1400, 1500, 1600°C, respectively. These specific materials were sintered with 8wt% yttria, at 2 GPa pressure and held at temperature for 10 minutes

Triphasic nanocomposites Si_3N_4/SiC/BN

Si-B-C-N ceramics are known to be thermally stable up to 2000°C. In spite of the amount of effort devoted by the scientific community to Si-B-C-N, bulk nanocomposites haven't been successfully processed until now.

The FTIR spectra of the as-crosslinked (at 400°C) precursor powders with varied doping are shown in Fig. 9(a). Aside from absorption bands that are inherited from the network of the polyureasilazane precursor, two boron-related bands can be observed, one is located at about 2505 cm-1, this is the stretching band of B-H bond. Another rather broadband that appears at 3130-3250 cm-1 range corresponds to B-OH. Addition of decaborane to the polyureasilazane precursor mainly brings about increase in B-H and B-OH absorption. B-H band starts to manifest when the decaborane addition is 5wt%, while a distinct B-OH band can only be seen when the percentage of decaborane exceeds 10wt%. With increasing doping, a broad absorption can be observed at 1250-1550 cm-1. This absorption corresponds to B-N bonding, according to the analogy of the structure to h-BN. After pyrolysis, the skeleton vibration of B-N is clearly seen in the FTIR spectra of samples containing higher B contents (Fig. 9(b)).

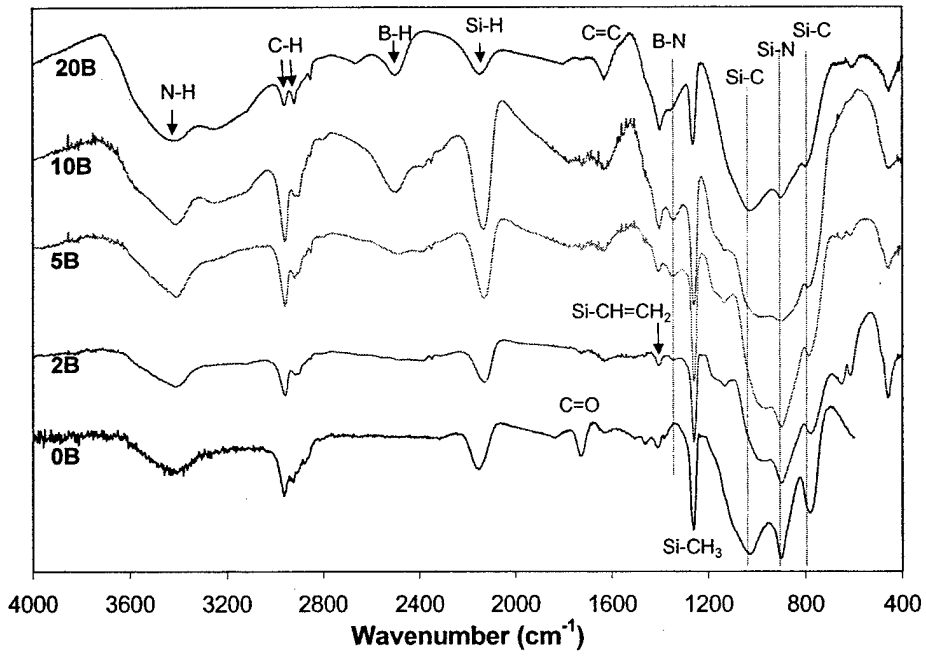

(a)

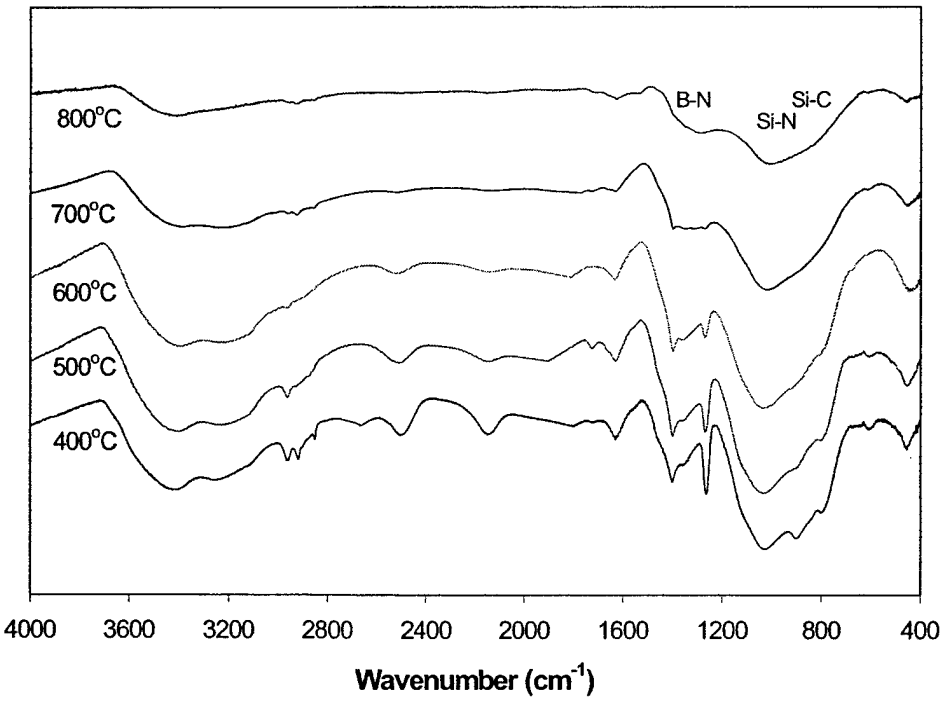

(b)

Fig. 9 FTIR spectroscopy showing absorption of (a) the 400°C-cross-linked polymers with different decaborane addition (b) evolution of bondings during pyrolysis of the 20wt% decaborane sample

Crystallization behavior of B-doped ceramics

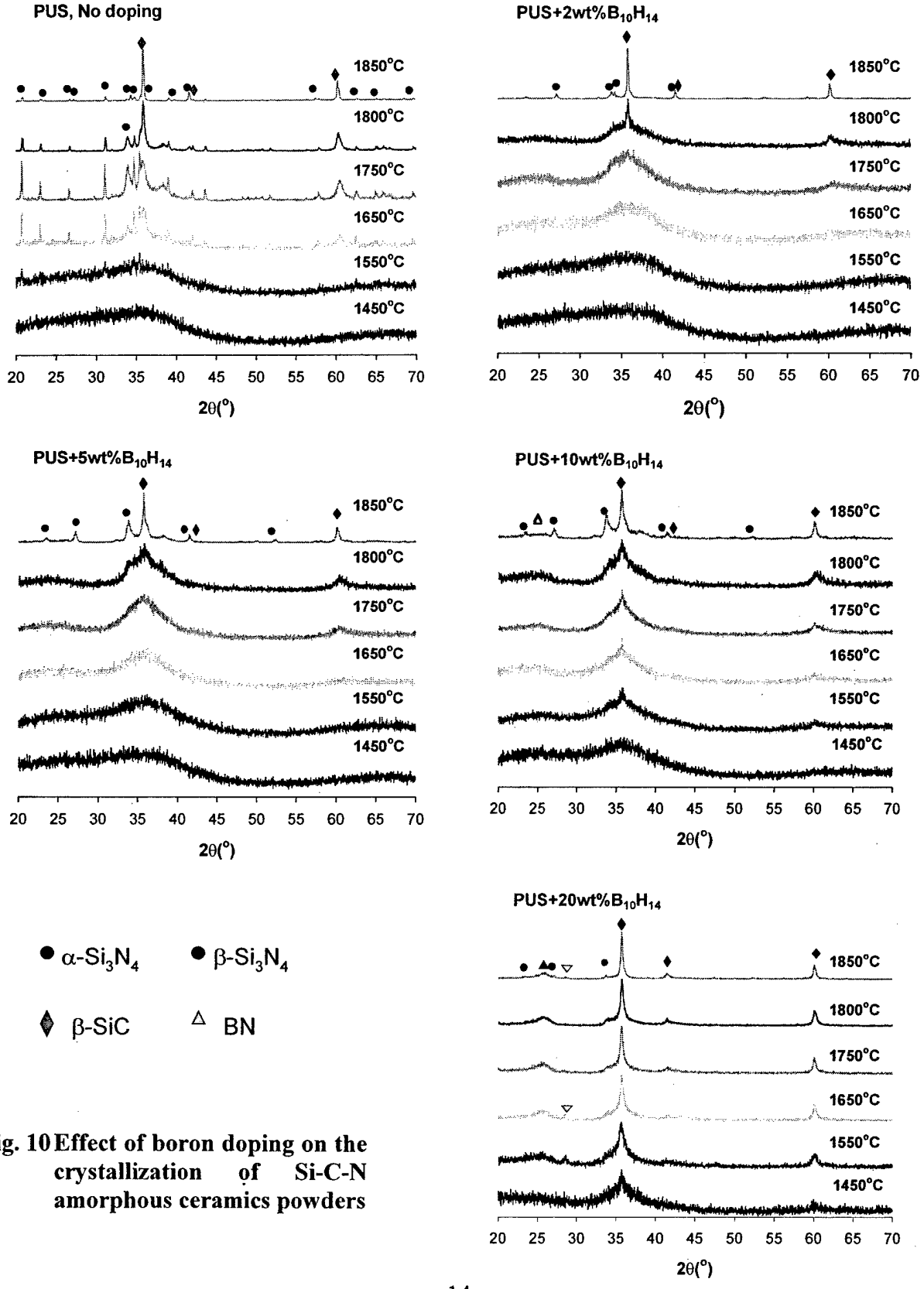

Fig. 10 Effect of boron doping on the crystallization of Si-C-N amorphous ceramics powders

The doping greatly enhanced the resistance to crystallization and thermal decomposition of the amorphous ceramics. As Fig. 10 indicates, 2wt% decaborane doping is enough to bring the crystallization on-set temperature from 1550°C up to 1800°C. The stabilization effect is roughly unchanged between 2-10wt% decaborane, indicating a wide window for the doping to be effective. When doped with higher than 10wt% decaborane, e.g., 20wt%, the crystallization temperature decreases severely to around 1450°C.

SPS production of the Si_3N_4/SiC/BN Nanocomposite

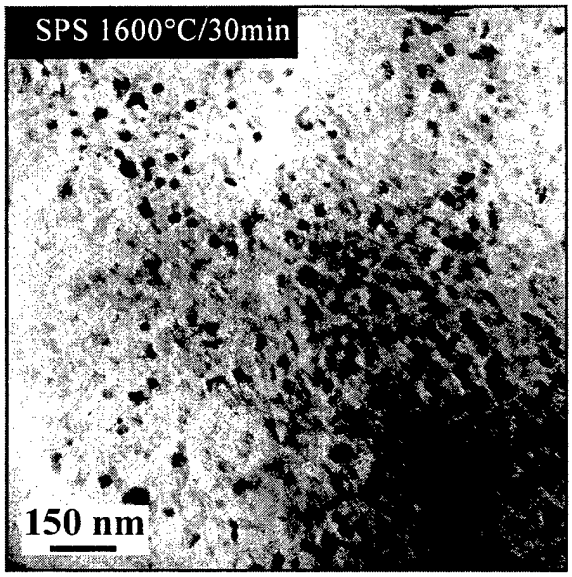

(a)

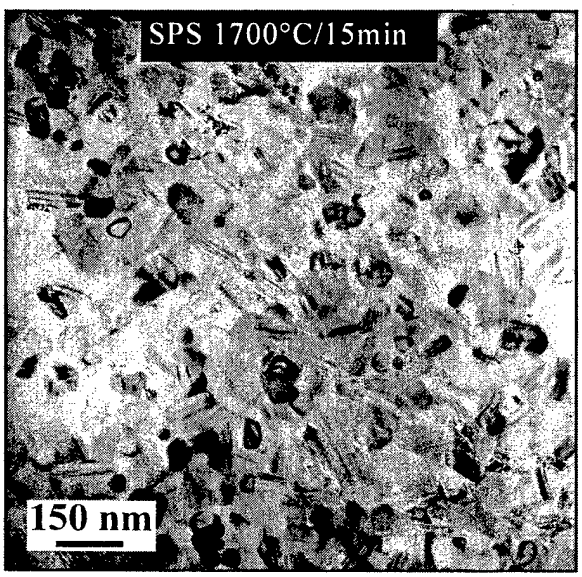

(b)

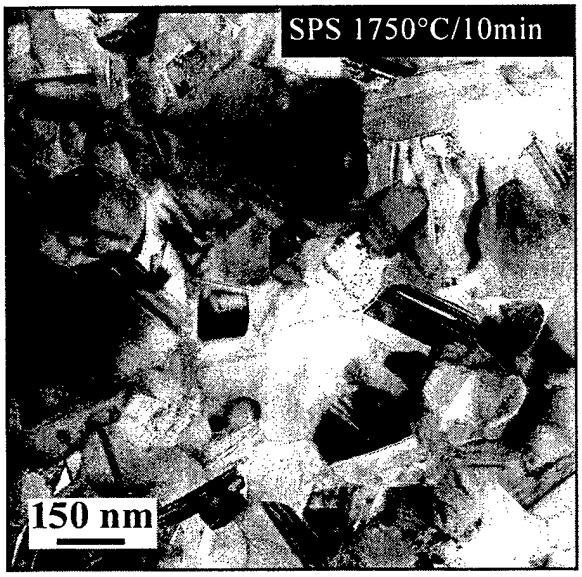

(c)

Fig. 11 SPS-derived nanocomposites of Si_3N_4/SiC/BN, these are the first sintered forms of the material. The precursor was doped with 10wt% decaborane in these cases

Amorphous Si-B-C-N powders derived from pyrolysis of the doped polymer precursors were sintered at 1600-1800°C by SPS. No sintering additives were involved in the consolidation.

Concurrent crystallization happens during sintering, leading to nanocrystalline composites of Si_3N_4/SiC/BN. Examples of the triphasic nanocomposites are shown in Fig.11. Depending on sintering temperature, the microstructure can be either nano-nano type or micro-nano type. SPS at 1600°C for 30 minutes leads to nano-nano type composite with grain size of about 25 nm; comparing Fig. 11(a) with Fig. 5, the presence of BN results in smaller grain size. Sintering at 1700°C/15min the grain size is larger while the nano-nano morphology is retained. While when the temperature is raised to 1750°C, the mean grain size grows further although the sintering time is shorter (10 min). In this case, some of the silicon nitride grains contain nano-SiC inclusions, which makes this material a micro-nano type composite.

The EELS mapping in Fig 12 conducted on microstructure similar to Fig. 11(b) indicates that the BN phase exists more as isolated blocks rather than a continuous layer that surrounds the other crystalline phases. Fig. 12 also reveals the location of oxygen in the material, which is mostly at triple junctions and also grain boundaries. HRTEM revealed that grain boundaries in the nanocomposites could be either with a thin glassy layer or be glass-free. BN (turbostratic, often co-exists with graphitic carbon) can be seen at the intergranular regions, as in Fig. 13.

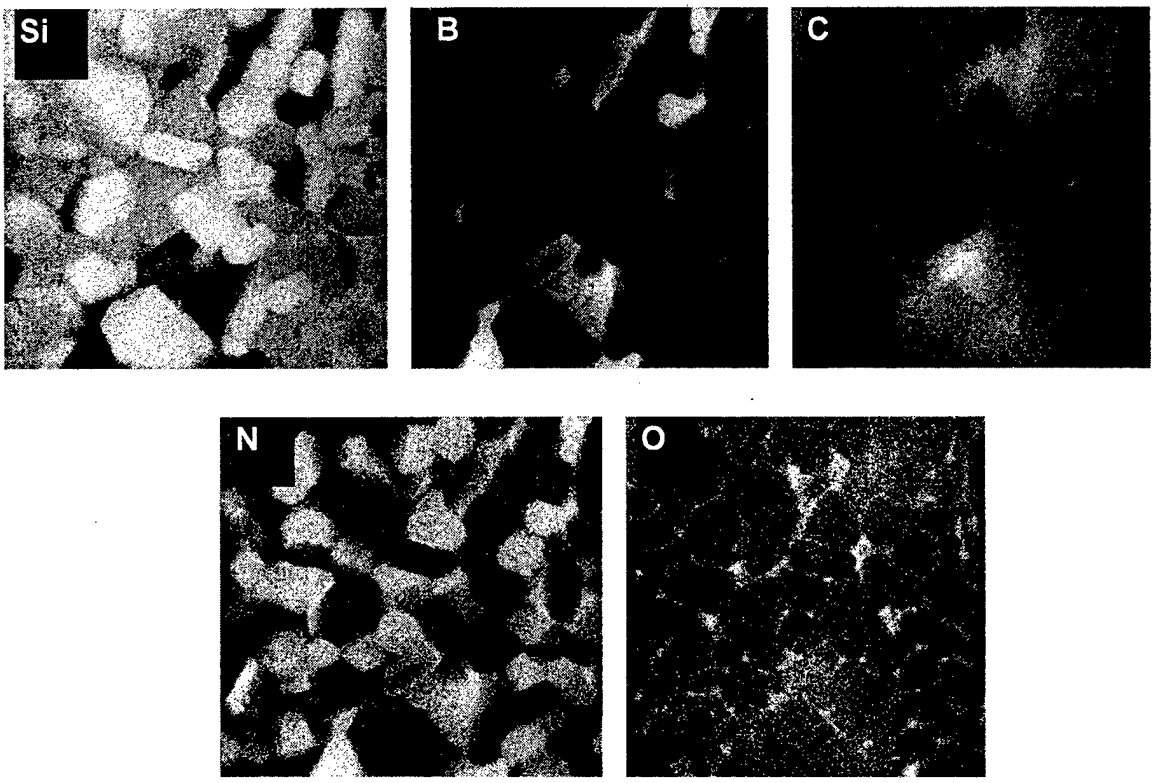

Fig. 12 Electron Energy Loss Spectroscopy of the Si_3N_4/SiC/BN nanocomposite

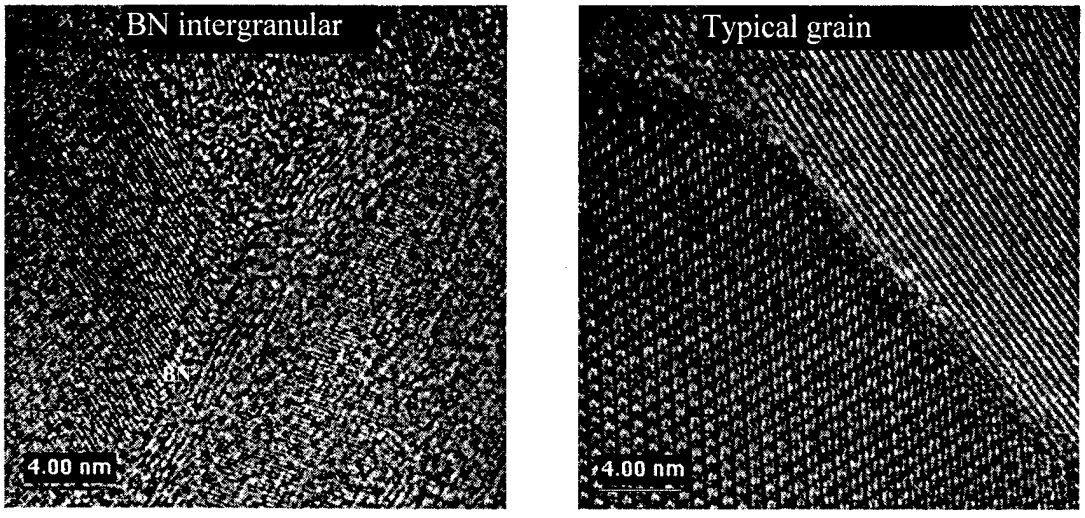

Fig. 13 HRTEM of the grain boundary characteristics of the triphasic nanocomposites

Creep property of nanocomposites

Compression creep curves measured by tests (in the temperature range 1400-1450°C and stress levels 50-200MPa) of one of the nano-nano composites, which contains 1wt% Y_2O_3 and sintered by SPS at 1600°C for 10minutes is shown in Fig. 14. The nano-nano composites show very high creep resistance, which is marked by their very low creep rate. The stress exponent is about unity, and the creep is featured by a very low activation energy of about 205 kJ/mol. The lack of oxide additive, which leads to unique grain boundary chemistry, has indeed brought about a fundamental change in the creep mechanism of the material.

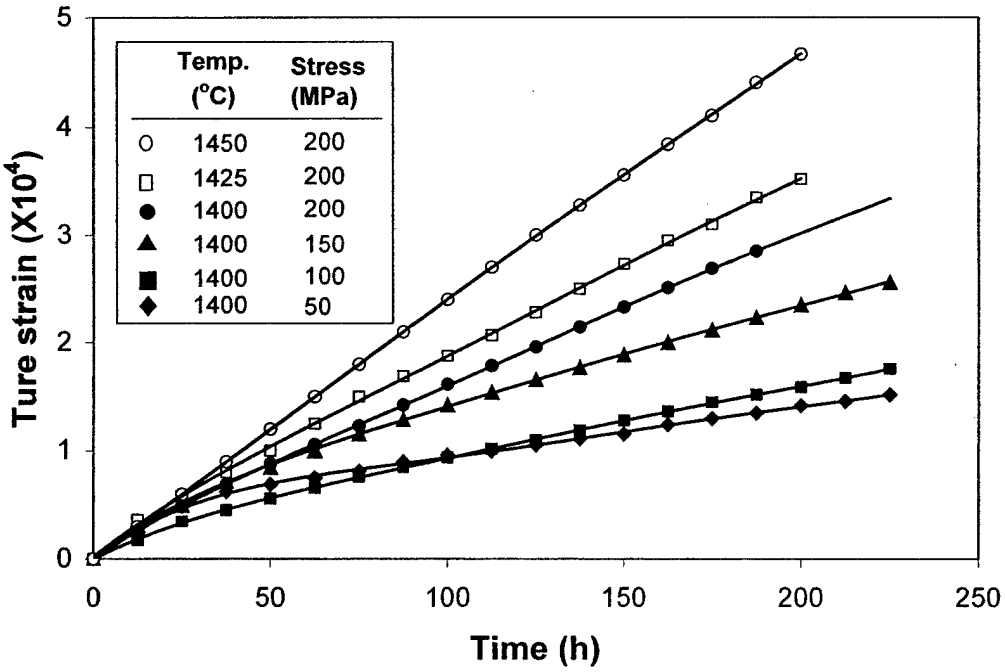

Fig. 14 Creep deformation of the nano-nano composite with low additive level (1wt% Y_2O_3)

Some of the measured steady state creep rates for the nanocomposites were compared with available data from literature in an effort to evaluate the merits of new nanocomposites against the existing silicon nitride materials in terms of creep property. Only compression creep data were selected in order to prevent the complication brought about by cavitation in tensile or bending test. The data measured at different temperature and stress levels were normalized to the reference condition (1400°C/100MPa) and plotted in Fig. 15. Group A is composed of silicon nitride ceramics (including silicon nitride/silicon carbide microcrystalline composites) with a high level of additive amounts (various additives are used by different researchers, as indicated

in the legend of this plot), most were sintered by hot-pressing. This group has the lowest creep resistance of the silicon nitride ceramics. For example, the steady state creep rate at the reference test condition 1400°C /100MPa ranges from about 3×10^{-8} to 3×10^{-6} 1/s. Using high purity silicon nitride powder, incorporation of less additive (e.g., less than 4wt%Y_2O_3), and applying hot-isostatic pressing or gas pressure sintering generates silicon nitride ceramics of higher creep property, which are included in Group B. These ceramics show secondary creep rate of about 1×10^{-9} to 3×10^{-8} 1/s, roughly two orders of magnitude lower than Group A. The micro-nano composites made by the present work with an approximately similar level of additive as Group

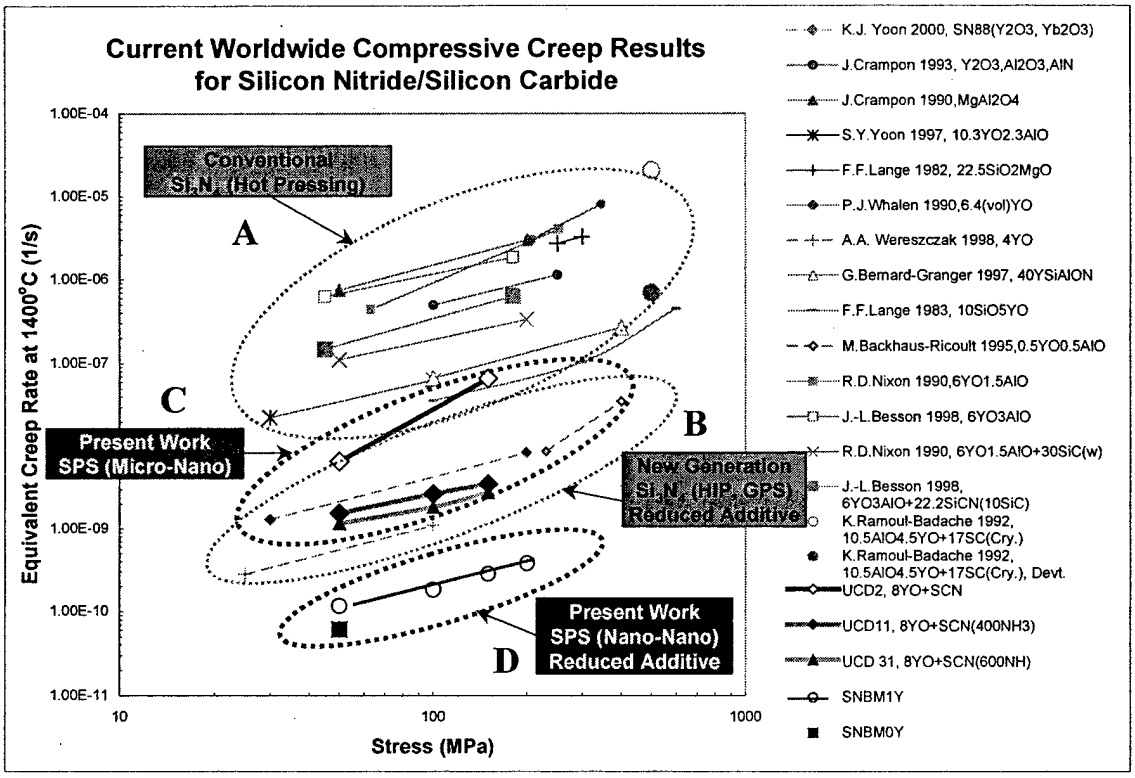

Fig. 15 Comparison of the creep resistance of the nanocomposites with other existing silicon nitride ceramics

A, which are shown in Fig. 15 as Group C, exhibit creep resistance superior to Group A but inferior to Group B. The nano-nano composites, however, demonstrate the highest creep resistance of all, as shown in Group D in Fig. 15. At the reference testing condition of 1400°C/100MPa, the steady-state creep rate of the nanocomposite sintered with 1wt%Y_2O_3 is about 1.67×10^{-10} 1/s, while the nanocomposite sintered without additive shows a creep rate of as low as 6.3×10^{-11} 1/s at 50MPa stress.

Regardless of specific creep mechanism, creep rate always has an inverse power of dependence on grain size for a certain creep mechanism. Which means if the creep mechanism remains the same, the smaller the grain size, the higher the creep rate should be. The extremely low creep rate of the nano-nano composites strongly suggests a completely different creep mechanism in these materials.

Summary

Major achievements are in the following aspects:

- Using concurrent crystallization during spark plasma sintering (SPS) of polymer-derived amorphous Si-C-N, both micro-nano and nano-nano type composites of silicon nitride and silicon carbide have been produced. The nano-nano composites are the first of its kind in the silicon nitride system that have been consolidated.
- For the first time, Si_3N_4/SiC nanocomposite has been consolidated without using oxide additive.
- Also for the first time, Si3N4/SiC/BN triphasic nanocomposites, which have extraordinarily high stability at high temperatures, were successfully developed in sintered form.
- Si3N4/SiC nano-nano composites were developed by high pressure sintering, these materials have a strong potential for high strain-rate superplastic forming.
- The nano-nano composites produced by SPS route of this project show the best creep resistance observed in silicon nitride materials examined so far. At 1400°C over a significant range of stresses, the experimentally measured creep rate is so low that we are reading the limit of our transducer resolution.

  The extraordinarily low creep rate was obtained by primarily minimizing the presence of intergranular glassy phase. This enabled the manifestation of diffusional process where the activation energy for grain boundary diffusion in such highly covalent solids can manage to manifest itself. Dislocation creep did not play any role in these studies.